Journal of Nuclear Materials 544 (2021) 152683

Contents lists available at ScienceDirect

Journal of Nuclear Materials

journal homepage: www.elsevier.com/locate/jnucmat

Implementation and Validation of the Hydride Nucleation-Growth-Dissolution (HNGD) model in BISON

Florian Passelaigue[a,*], Evrard Lacroix[c], Giovanni Pastore[b,d], Arthur T. Motta[a]

[a] Ken and Mary Alice Lindquist Department of Nuclear Engineering, The Pennsylvania State University, University Park, PA 16802, USA
[b] Computational Mechanics and Materials Department, Idaho National Laboratory, Idaho Falls, ID 83415, USA
[c] Framatome Inc., 3315 Old Forest Rd, Lynchburg, VA 24501
[d] Department of Nuclear Engineering, University of Tennessee, Knoxville, TN 37916, USA

ARTICLE INFO

Article history:
Received 8 September 2020
Revised 4 November 2020
Accepted 12 November 2020
Available online 22 November 2020

Keywords:
Nuclear material
Zircaloy
Zirconium hydride
HNGD
BISON

ABSTRACT

During the operation of a light water reactor, a fraction of the hydrogen produced by waterside corrosion is absorbed into the nuclear fuel cladding. When the hydrogen concentration reaches its solubility limit, a brittle zirconium hydride phase precipitates, leading to a loss of ductility of the cladding. To assess cladding integrity, an accurate simulation tool is needed to predict hydrogen distribution within the cladding and hydride precipitation. Recent studies have developed an improved understanding of the physical processes involved in hydrogen redistribution, and hydride precipitation and dissolution. This research led to the development of a new model, called Hydride Nucleation-Growth-Dissolution (HNGD). The present work describes the implementation of HNGD into the fuel performance code BISON, developed at Idaho National Laboratory. The main innovative feature of the HNGD model is that it accounts for hydride nucleation and growth as two distinct precipitation components, using the Johnson-Mehl-Avrami-Kolmogorov model to describe hydride growth kinetics. Each step of the model implementation into BISON was systematically verified, and simulations of experiments performed for validation, showing that the HNGD model provides improved predictions, and captures some experimentally observed physical phenomena related to hydride growth that the previous model could not.

1. Introduction

During operation of a light water reactor, waterside corrosion leads to hydrogen pickup into the Zr alloy cladding tube, as illustrated schematically in the first panel of Figure 1. The hydrogen redistributes in the cladding following temperature, stress and concentration gradients into regions of low temperature, high stress and low concentrations (Fig. 1, second panel). When the local concentration reaches the solubility limit, a zirconium hydride phase precipitates [1].

This brittle hydride phase can compromise cladding integrity, so simulation tools able to predict accurately hydrogen redistribution and hydride precipitation and dissolution are needed. A simplified model was implemented into the fuel performance code BISON developed at Idaho National Laboratory (INL) [2,3], but recent work brought an improved understanding of the physics involved in hydride precipitation and dissolution [4]. Following this new understanding, a new model called Hydride Nucleation-Growth-Dissolution (HNGD) has been developed. Figure 2 shows a schematic comparison between HNGD and the model previously used in BISON. The precipitation and dissolution of hydrides depends on the temperature and on the hydrogen content in solid solution. In the previous model, precipitation occurs when the matrix is oversaturated with hydrogen, but stops when the precipitation limit is reached. The limit considered here is the so called Terminal Solid Solubility for Precipitation (TSS_P). Hydrides dissolve if they exist in a matrix that is undersaturated in hydrogen. The saturation limit is known as the Terminal Solid Solubility for Dissolution (TSS_D), and the dissolution is considered instantaneous. According to that model, between TSS_P and TSS_D there is a hysteresis region in which neither hydride precipitation nor dissolution occurs.

In the HNGD model however, hydride precipitation is divided into nucleation of new hydrides and growth of existing ones. Because of this a marked difference occurs when there are pre-existing hydrides upon cooling and when all the hydrogen is dissolved: experimential evidence shows that hydrides can grow while being held in the hysteresis region at constant temperature [5]. Nucleation of new hydrides occurs when the solid solution content is above the TSS_P. The TSS_D is identified as the

* Corresponding author.
E-mail address: fpp8@psu.edu (F. Passelaigue).

https://doi.org/10.1016/j.jnucmat.2020.152683
0022-3115/

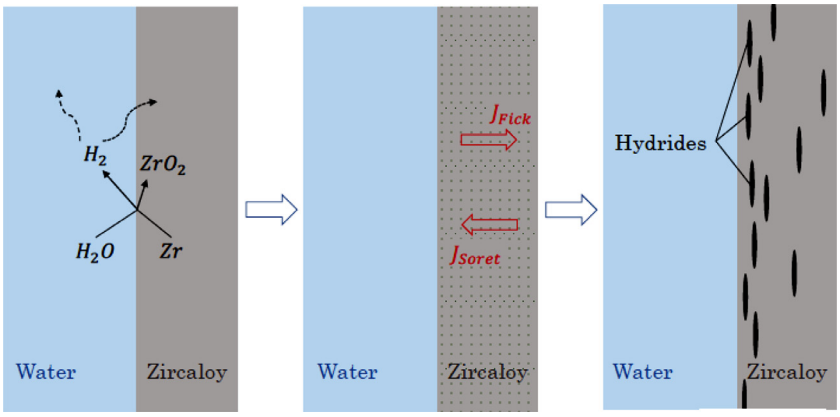

Fig. 1. Schematic representation of the hydriding process. Waterside corrosion of the Zircaloy causes hydrogen absorption. This hydrogen is distributed by Fick's law and Soret effect, and a high hydrogen content leads to zirconium hydride precipitation.

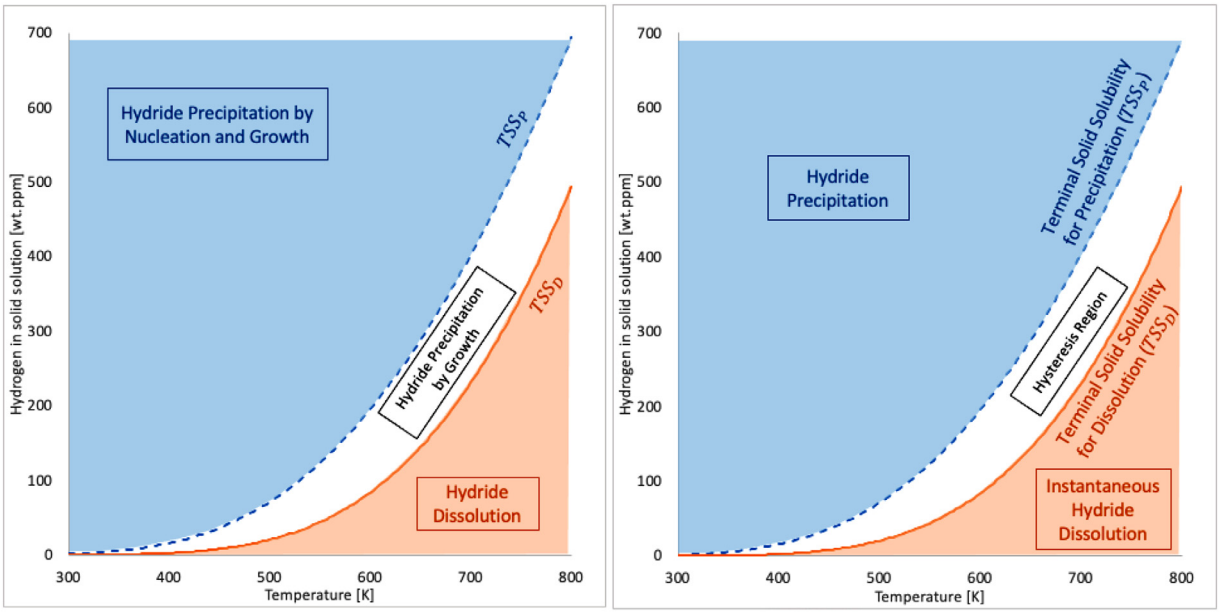

Fig. 2. Hydrogen concentration (in [wt.ppm], equivalent to [μg/g]) versus temperature. Illustration of the HNGD model (a) [4], compared with the model previously used in BISON (b) [2,3]. The hydrogen precipitation behavior is determined by the temperature and hydrogen solid solution content conditions. The previous model considers that (i) precipitation occurs when the solid solution content is in the blue region either by cooling or by increase in hydrogen concentration (above the TSS_P curve), (ii) dissolution happens instantaneously under the TSS_D curve, and (iii) between the two is a hysteresis zone where neither precipitation or dissolution occurs. The HNGD model considers that in the blue region, hydride precipitation occurs by nucleation and growth, and in the white region, hydride precipitation occurs by hydride growth only so that a hysteresis region does not exist. Hydride nucleation and growth can take place simultaneously. Moreover, hydride dissolution is no longer considered to be instantaneous.

thermodynamic solubility limit while the TSS_P is identified as the supersolubility limit [4]. The growth of existing hydrides occurs when the solid solution content is above the TSS_D. The kinetics of precipitation by hydride growth are described using the Johnson-Mehl-Avram-Kolmogorov (JMAK) model [6]. Both of these precipitation mechanisms occur at specific rates, determined by kinetic parameters. Further, in the HNGD model hydride dissolution is no longer considered instantaneous [4]. These three phenomena are described by Equations (1) to (3):

$$Dissolution: \frac{\partial C_{SS}}{\partial t} = -K_D(C_{SS} - TSS_D) \quad (1)$$

$$Nucleation: \frac{\partial C_{SS}}{\partial t} = -K_N(C_{SS} - TSS_P) \quad (2)$$

$$Growth: \frac{\partial C_{SS}}{\partial t} = -K_G(C_{tot} - TSS_D)p(1-x)(-ln(1-x))^{1-1/p} \quad (3)$$

where C_{SS} is the hydrogen content in solid solution, K_D, K_N, K_G are the kinetic parameters for dissolution, nucleation and growth respectively, $x = \frac{C_{tot}-C_{SS}}{C_{tot}-TSS_D}$ is a measure of the advancement of the precipitation reaction, with C_{tot} the sum of the hydrogen contents in solid solution and in hydrides, and p is the dimensionality of the growth (in the JMAK model $p \sim 2.5$ for platelets). [6]

In the zirconium alloy cladding, hydrogen atoms migrate principally driven by a concentration gradient (Fick's diffusion) and by a temperature gradient (Soret effect). These two effects modify the hydrogen concentration in solid solution as per Equation (4):

$$\frac{\partial C_{SS}}{\partial t} = -\nabla\left(-D\nabla C_{SS} - \frac{DQ^*C_{SS}}{RT^2}\nabla T\right) \quad (4)$$

where D is the hydrogen diffusion coefficient in the material (following an Arrhenius law), Q^* is the heat of transport of hydrogen in zirconium (assumed not to vary with temperature) and R is the ideal gas constant.

Table 1
Parameters of the HNGD model [4,5]

Parameter	Symbol	Value
Preexponential term and activation energy of the supersolubility Arrhenius law (Eq. (5))	TSS_{P0}	3.08×10^4 $wt.ppm$
	Q_P	0.26 $eV.at^{-1}$
Preexponential term and activation energy of the solubility Arrhenius law (Eq. (5))	TSS_{D0}	1.02×10^5 $wt.ppm$
	Q_D	0.37 $eV.at^{-1}$
Preexponential term and activation energy of the diffusion coefficient Arrhenius law	D_0	1.08×10^{-2} $cm^2.s^{-1}$
	E_D	0.46 $eV.at^{-1}$
Preexponential terms of the nucleation, dissolution reaction-controlled growth and diffusion-controlled growth kinetics Arrhenius laws (Eqs. (6) to (8))	K_{D0}	1.11×10^3 s^{-1}
	K_{N0}	2.75×10^{-5} s^{-1}
	K_{th0}	5.35×10^5 s^{-1}
	K_{mob0}	1.6×10^{-5} s^{-1}
Coefficients of the 3rd degree polynomial used to express the formation energy of δ hydrides (Eq. (9))	E_{th0}	5.66×10^{-1} $eV.at^{-1}$
	E_{th1}	4×10^{-4} $eV.at^{-1}.K^{-1}$
	E_{th2}	2×10^{-7} $eV.at^{-1}.K^{-2}$
	E_{th3}	3×10^{-10} $eV.at^{-1}.K^{-3}$
Activation energy of the diffusion-controlled growth kinetics Arrhenius laws (Eq. (3))	E_G	0.9 $eV.at^{-1}$
Heat of transport of hydrogen in zirconium.	Q^*	0.26 $eV.at^{-1}$

2. HNGD Parameters

In the HNGD model the solubility limits discussed above are fitted using Arrhenius-type laws (Eq. (5))

$$\begin{aligned} TSS_D &= TSS_{D0} \times exp\left(\frac{-Q_D}{RT}\right) \\ TSS_P &= TSS_{P0} \times exp\left(\frac{-Q_P}{RT}\right) \end{aligned} \tag{5}$$

where the preexponential factors TSS_{D0}, TSS_{P0} and activation energies Q_D, Q_P are determined empirically [7–12].

The hydride dissolution and nucleation K_D and K_N kinetic parameters also follow Arrhenius laws. Hydride growth can be limited by two factors: hydrogen diffusion (subscript 'mob' for mobility) and matrix/hydride interface reaction (subscript 'th' for thermodynamics). Each of these contributions follows an Arrhenius law. These three factors are described in Equations (6) to (8). [4]

$$Dissolution : K_D = K_{D0} exp(-\frac{E_D}{RT}) \tag{6}$$

$$Nucleation : K_N = K_{N0} f_\alpha exp(-\frac{E_{th}}{RT}) \tag{7}$$

$$\begin{aligned} Growth : & \left.\begin{array}{l} Diffusion\ controlled : \ K_{mob} = K_{mob0} f_\alpha v_0 exp(-\frac{E_G}{RT}) \\ Reaction\ controlled : \ K_{th} = K_{th0} f_\alpha v_0 . exp(-\frac{E_{th}}{RT}) \end{array}\right\} \\ & K_G = (1/K_{mob} + 1/K_{th})^{-1} \end{aligned} \tag{8}$$

where K_{D0}, K_{N0}, K_{mob0}, K_{th0} are the preexponential factors of the Arrhenius laws for dissolution, nucleation, diffusion-controlled growth, and reaction-controlled growth; E_D is the activation energy for diffusion of hydrogen in Zircaloy; E_G is the activation energy for hydride growth by accretion of hydrogen atoms to the particle by diffusion, the coefficients f_α and v_0 are defined below, and E_{th} is the formation energy of the hydride, fitted with a degree 3 polynomial (Eq. (9)). The coefficients are given in Table 1.

$$E_{th} = -E_{th0} + E_{th1} T - E_{th2} T^2 + E_{th3} T^3 \tag{9}$$

The dependencies on hydride content are described by:

- Volume fraction of α phase:

$$f_\alpha = 1 - \frac{x_{Prec}}{x_\delta - x_\alpha}$$

- Atomic fraction of hydride (with M_H and M_{Zr} the atomic weights of hydrogen and zirconium, C_{prec} the precipitated hydride content, and C_{tot} the total hydrogen content in $wt.ppm$):

$$x_{Prec} = \frac{C_{Prec}}{M_H(\frac{C_{Prec}}{M_H} + \frac{10^6 - C_{Prec}}{M_{Zr}})}$$

- Atomic fraction of hydrogen at the $(\delta/\alpha + \delta)$ boundary: [4,5]

$$x_\delta(T) \approx -9.93 \times 10^{-11} T^3 + 8.48 \times 10^{-8} T^2 - 5.73 \times 10^{-5} T + 0.623$$

- Atomic fraction of hydrogen in the α phase:

$$v_0 = \frac{x_0 - x_\alpha}{x_\delta - x_\alpha}$$

- Atomic fraction of hydrogen (total):

$$x_0 = \frac{C_{tot}}{M_H(\frac{Ctot}{M_H} + \frac{10^6 - Ctot}{M_{Zr}})}$$

- Atomic fraction of hydrogen in the α phase:

$$x_\alpha = \frac{TSS_D}{M_H(\frac{TSS_D}{M_H} + \frac{10^6 - TSS_D}{M_{Zr}})}$$

The default values of the parameters are shown up in Table 1. These come from the original development of the HNGD model in [4,5].

3. BISON update

3.1. HNGD Model Verification

3.1.1. Analytical Verification

The HNGD model described in the previous section is implemented in BISON, the finite element based nuclear fuel performance code developed at INL. As mentioned earlier, each phenomenon was systematically verified. Hypothetical cases are used to check the mathematical behavior of the model.

The hydride dissolution verification case assumes a uniform sample of Zircaloy loaded with $C_{tot} = 250 wt.ppm$ of hydrogen, maintained at a constant temperature of $550K$. At this temperature, the equilibrium concentration of hydrogen in solid solution is $TSS_D^{550} = 44 wt.ppm$. Using the initial condition $C_{SS}(0) = 0 wt.ppm$ (i.e. all hydrogen is in hydride particles) the analytical solution of Equation 1 is given by Equation 10:

$$C_{SS}(t) = TSS_D^{550}(1 - e^{-K_D^{550} t}) \tag{10}$$

Because the concentration in solid solution is below the solubility limit, the hydrides dissolve and C_{SS} increases exponentially to reach the equilibrium value. Figure 3a shows the difference between the analytical solution in Equation 10 and the computed result for various time step values. The computed solution follows well the measured precipitation kinetics and approaches the predicted equilibrium value from the analytical solution. Also, as expected, the difference decreases when the time step is reduced.

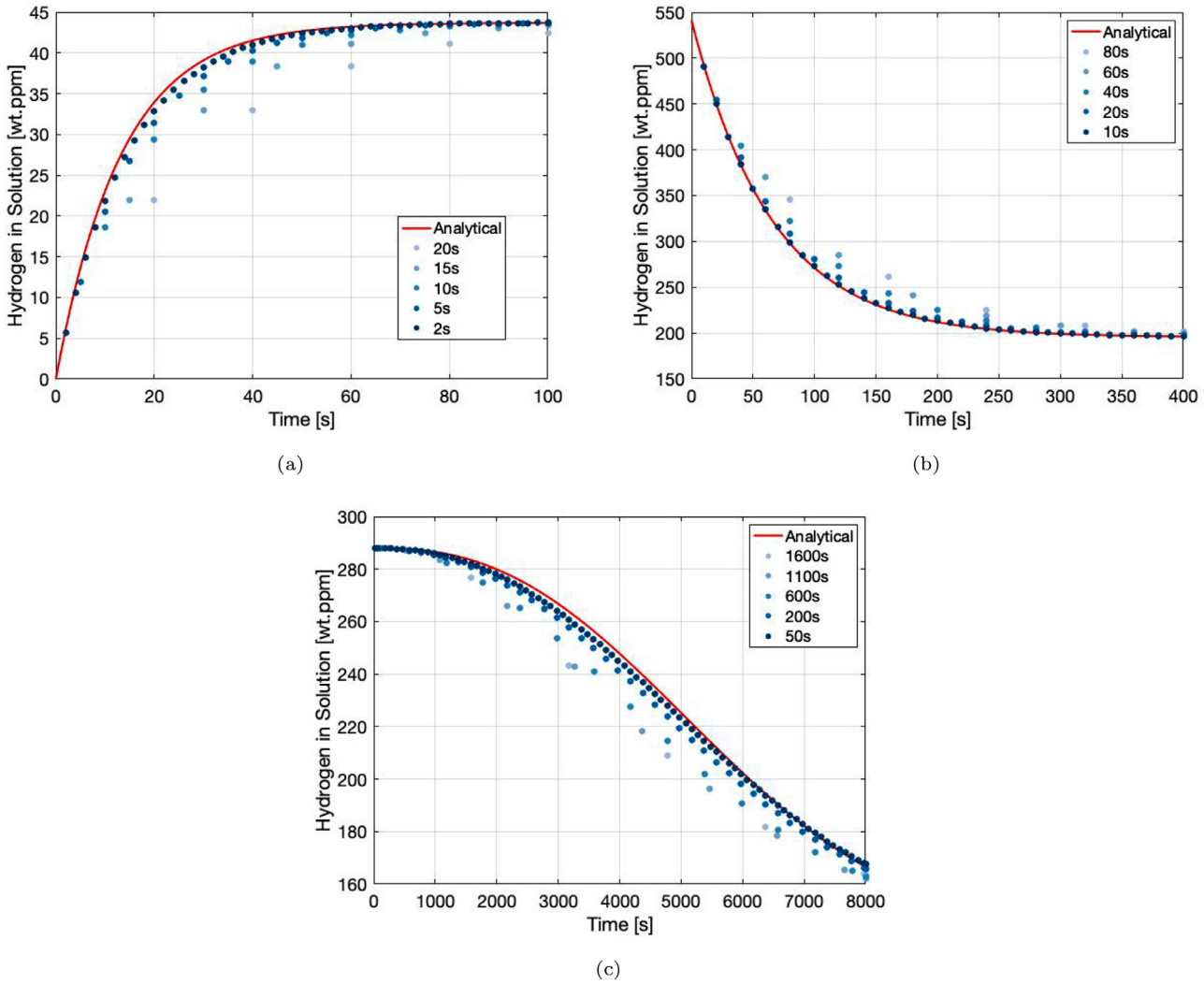

Fig. 3. Verification of (a) hydride dissolution, (b) hydride nucleation and (c) hydride growth computation in BISON using HNGD. The computed results for the hydrogen concentration in solid solution are compared to the analytical solutions for different time step values. As the time step is reduced, the computed result converges to the analytical solution.

The hydride nucleation verification studies a case of Zircaloy uniformly loaded with $C_{tot} = 540wt.ppm$ of hydrogen, maintained at a constant temperature of $600K$. At this temperature, the equilibrium concentration of hydrogen in solid solution for nucleation only is $TSS_P^{600} = 195wt.ppm$ (we turn off the growth term in the model for this calculation so no growth is computed here). At this hydrogen level, the factor f_α from Equation 7 is close to 1 and does not vary significantly during the computation. Assuming this value is constant and equal to 1 and using the initial condition $C_{SS}(0) = C_{tot}$ (i.e. all hydrogen is in solid solution) the analytical solution to Equation 2 is given by Equation 11:

$$C_{SS}(t) = TSS_P^{600} + (C_{tot} - TSS_P^{600})e^{-K_N^{600}t} \tag{11}$$

Because the hydrogen concentration in solid solution is above the TSS_P, the solid solution content decreases exponentially until it reaches the TSS_P. As previously, Figure 3b shows the computed results and the analytical solution, illustrating that the calculated results reproduce the nucleation well and the difference between analytical and calculated hydrogen content decreases when the time step is reduced.

The hydride growth verification case assumes a uniform sample of Zircaloy loaded with $C_{tot} = 288wt.ppm$ of hydrogen, maintained at a constant temperature of $650K$. At this temperature, the equilibrium concentration of hydrogen in solid solution is $TSS_D^{650} = 144wt.ppm$. As before, f_α and ν_0 (in Eq. 8) are assumed to be equal to 1. Using the initial condition $C_{SS}(0) = C_{tot}$ (i.e. all hydrogen is in solid solution) the analytical solution to Equation 3 is given by Equation 12. In this case, the hydride nucleation computation is disabled, so in the code the hydride content is actually initialized at $10^{-6}wt.ppm$ so the algorithm triggers the hydride growth computation, and we have hydride precipitation by pure hydride growth.

$$C_{SS}(t) = TSS_D^{650} + (C_{SS}(0) - TSS_D^{650})e^{-(K_G^{650}t)^p} \tag{12}$$

The convergence of the computed results of hydrogen in solid solution with decreasing time step values is illustrated in Figure 3c. The kinetics of hydride precipitation by hydride growth only is well reproduced by the model. Again, the difference between simulation and analytical solution decreases with decreasing time step values.

3.1.2. Uniform-Temperature Sample Behavior

Each of the verification cases described above features one phenomenon of the HNGD model, occuring at one temperature. This section shows the behavior of a sample uniformly loaded with $200wt.ppm$ of hydrogen, which is subjected to a heat treatment consisting of a heat-up followed by a cool-down. Two cases are differentiated, whereby hydrides are completely dissolved at the end

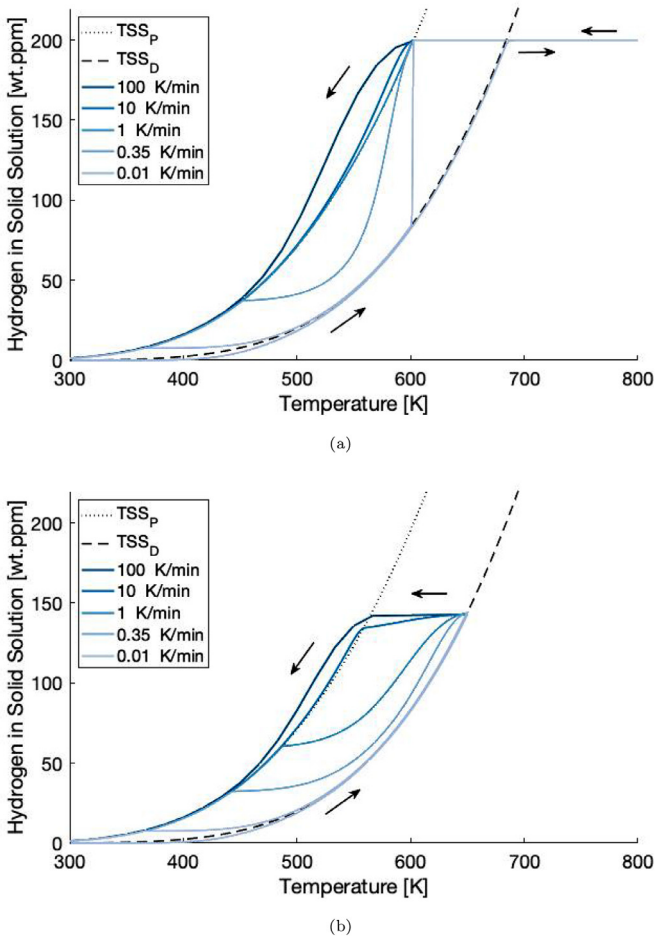

Fig. 4. Influence of cooling rate on hydride precipitation for total (a) and partial (b) dissolution in a sample containing $200wt.ppm$. The model show deviations from the TSS_P and TSS_D curves values at higher cooling or heating rates, as observed experimentally [4]. It also provides insight on deviations below the TSS_P at cooling rates lower than $0.35K/min$

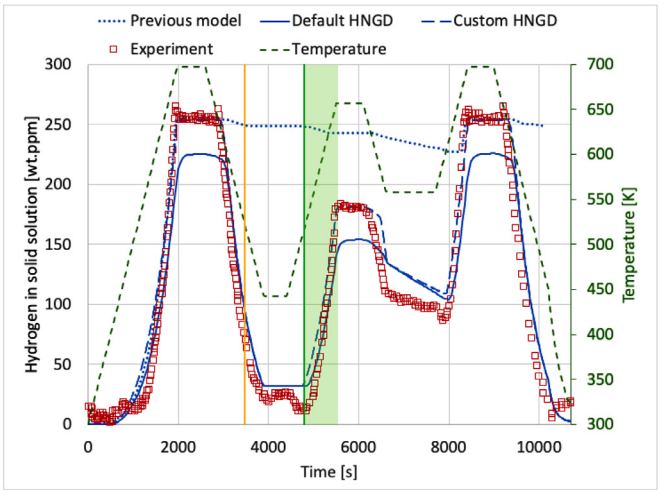

Fig. 5. Thermal transients benchmark [4]. A hydrogen-loadded sample is submitted to a thermal treatment (green) and the evolution of the hydrogen concentration is recorded (red squares). This plot shows the comparison between the previous model (dotted blue line) and the HNGD model, using two different solubilities: default (full blue line) and fitted to this experiment (dashed blue line). The HNGD model leads to a marked improvement in the predictions.

of the heat-up phase or only partially. Each case was computed using a range of values for the cooling rate.

Figure 4 shows the calculated results of the hydrogen in solid solution in this sample when heated to $800K$ (complete dissolution, Fig. 4a) and to $650K$ (incomplete dissolution, Fig. 4b). Figure 4a shows that when the sample is heated to $800K$ all hydrogen goes into solid solution ($C_{SS} = 200wt.ppm$). Subsequent cooling causes no precipitation until the TSS_P is reached. At that point different results accrue depending on the cooling rate. At a $10K/min$ cooling rate, the concentration of hydrogen in solid solution follows closely the TSS_P curve, indicating that most hydrogen precipitates through hydride nucleation, which is fast enough to maintain its equilibrium at TSS_P while hydride growth is too slow to be significant. At very high cooling rates ($100K/min$), departure from the equilibrium behavior is clearly observed. In particular, as the hydride nucleation kinetics is not rapid enough to keep up with the temperature decrease, the concentration of hydrogen in solid solution is higher than the TSS_P during the transient. In contrast, for low cooling rate ($0.35K/min$ and below), hydrogen precipitation into hydrides occurs mostly by hydride growth. Accordingly, for the low cooling rates the curve deviates significantly from TSS_P and the hydrogen in solid solution decreases upon holding for a long time at a constant temperature.

In contrast, when some hydrides are still present at the highest temperature, hydrogen precipitation by hydride growth starts to occur immediately when the sample starts to be cooled (no need to reach TSS_P). Figure 4b shows the results for such simulation. The sample is heated up to $650K$. At this temperature the total hydrogen content is higher than the solubility, so there are still hydrides particles in the sample when the cool down begins (about $55wt.ppm$ of hydrogen is in precipitated form). The results show that hydrogen precipitation by hydride growth becomes increasingly important as the cooling rate decreases.

Thus the simulations in this section show that the HNGD model behaves as intended, as it is qualitatively consistent with the data presented in [5].

3.2. HNGD Model Validation

Now that the HNGD model is verified, it is tested by comparing its predictions with experiments. Three types of experiments are presented here. The first one uses a Zircaloy sample subjected to a uniform temperature treatment, which validates that the HNGD model is able to predict hydride precipitation. The second one uses a sample loaded with a uniform hydrogen distribution and subjected to a temperature gradient, which validates that the model is able to predict the hydrogen distribution in such setup. The third one uses a sample loaded with hydrogen via a hydride rim formed at one end, subjected to an asymmetric temperature profile. The results of the calculation shows that further work is needed to predict hydride precipitation on a broad region when the hydrogen is not uniformly distributed at the beginning of the experiment.

3.2.1. Transients Benchmark

The first experiment used for validation consist of a series of thermal transients applied to a hydrogen-loaded sample while the evolution of the hydrogen concentration is monitored via synchrotron X-ray diffraction [4]. The temperature changes lead to successive dissolution and precipitation. The $254wt.ppm$ sample is subjected to the heating and cooling cycle shown by the dashed line in Figure 5, which was designed to highlight the different phenomena occuring in the sample by inducing successive dissolution and precipitation [4]. The sample is initially at room temperature and is heated to $700K$, which is enough to dissolve all the hydrides; accordingly the hydrogen in solid solution increases to the full amount. In the following cycle, the temperature is raised

to 660K, which causes 180$wt.ppm$ to dissolve. The temperature is then held at 560K, causing the hydrogen in solid solution to decrease from 110$wt.ppm$ to 85$wt.ppm$ during a 1000s-temperature hold because of hydride growth. Then the sample is heated again to 700K, causing all the hydride particles to dissolve, and the sample is finally brought back to room temperature. These thermal transients are applied while the hydrogen in solid solution content is measured via the hydride diffraction signal [4]. Figure 5 shows the evolution of hydrogen content in solid solution, comparing the experimental data (red squares) with BISON using the previous model (dotted blue line) and the HNGD model, using two different fits for the solubility. In particular, the plain blue line uses the default fit of the model, while the dashed blue uses a custom TSS_D fit. The experimental data shows that there is a total dissolution of the hydrides by the end of the first heat-up. This is predicted by the previous BISON model, but the dissolution is only partial with the HNGD model using its default solubility fit. To provide an additional comparison to the previous BISON model that excludes the effect of a particular parameter, and thus isolate the impact of the new hypotheses of the HNGD model, an Arrhenius fit based on the first heat-up was used in the custom HNGD calculation. Given the variability of the TSS_D values in the litterature [7–12], this fit is still in the 1σ uncertainty range of the default fit.

The two models diverge during the first cool-down: at the yellow marker the solid solution concentration reaches the hysteresis region ($TSS_D < C_{SS} < TSS_P$) so the previous model stops the hydride precipitation, while the HNGD model continues to compute precipitation by hydride growth. Another difference occurs when the second heat-up starts, marked by the green line and shade. For the previous model the solid solution concentration is still high so it resumes precipitation ($C_{SS}^{previous} > TSS_P$) until the concentration in solid solution content reaches TSS_P. Instead, for the HNGD model, most of the hydrogen is in hydrides at that point, so hydride dissolution occurs ($C_{SS}^{HNGD} < TSS_D$) until reaching the solubility limit (TSS_D). It is clear that the HGND model provides a better description of the experimental data than the previous model.

The difference between the two solubility fits used by the HNGD model is particularly apparent at high temperature. Experimentally, all hydrogen is in solid solution at 700K, and the custom simulation is consistent with this, but there are still about 20$wt.ppm$ of hydride when using the default parameters. This leads to another difference happening at the beginning of the cool down. In the default simulation, hydride growth occurs as soon as the temperature starts decreasing, whereas the custom simulation must reach TSS_P to trigger hydride nucleation and start precipitating.

This validation case shows that the HNGD model is able to predict hydride precipitation and dissolution in a uniformly hydrided sample. The next section shows the ability to predict the hydrogen profile in a sample initially uniformly loaded with hydrogen and subjected to a temperature gradient for a long time.

3.2.2. Sawatzky's experiments

The second set of cases used for validation is Sawatzky's two experiments described in [13]: two 2.54cm long Zircaloy-2 samples loaded with hydrogen (130$wt.ppm$ and 63$wt.ppm$ respectively) are subjected to a temperature gradient (57.9K/cm and 116K/cm) for 34 and 41 days respectively. We use the HNGD model in BISON to simulate this couple of experiments and compare the hydrogen profile after 34 and 41 days respectively.

Figure 6 shows the result from BISON computation (blue) compared to the experimental data (red markers) and the analytical solution derived by Sawatzky (red line). This analytical solution was obtained based on the following assumptions: (i) the hydrogen is the only component diffusing, (ii) it diffuses mainly in the matrix, and (iii) the hydrogen in solution is in equilibrium with the hydride particles in the biphasic region (i.e. $C_{SS} = TSS_D$). See [13] for complete derivation. In Figure 6a, the additional grey curve represents the results using the previous model [3]. The shape of the profile is much closer to the analytical solution when computed with the HNGD model in BISON (the peculiar shape of the profile is discussed below). The hydride peak and steep limit between the one-phase and two-phase regions appear clearly, and the height and position of this peak are consitent with the data.

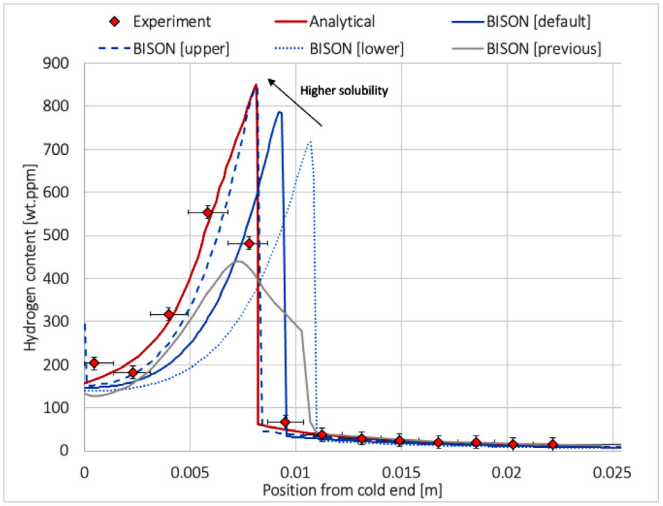

(a)

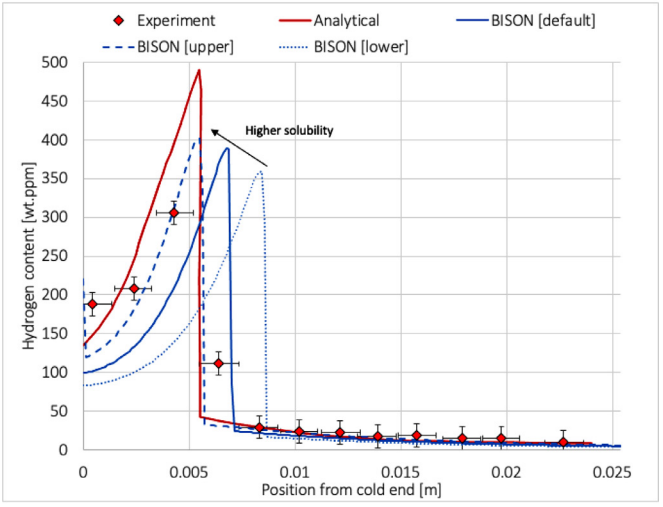

(b)

Fig. 6. Simulations of Sawatzky's experiments, compared with experimental data and analytical solution from [13]. The hydrogen contents are 130 $wt.ppm$ (a) and 64 $wt.ppm$ (b). The shape of the profile is much closer to the analytical solution that follows the data when using the HNGD model. The additional profiles [upper]/[lower] were obtained by using a solubility fit one standard deviation above and under the default value.

In order to perform an initial assessment of the sensitivity of the results to the model parameters, two additional simulations were made with different correlations of the solubility. Because the parameters TSS_{D0} and Q_D (Eq. (5)) were determined using the various values found in the literature [7–12], an estimation of the associated standard deviations can be made. The curves noted [upper] and [lower] are obtained with solubilities respectively higher and lower than the default one. The solubility fit impacts the position of the frontier between the biphasic and monophasic regions, as well as the height of the hydride peak at this limit.

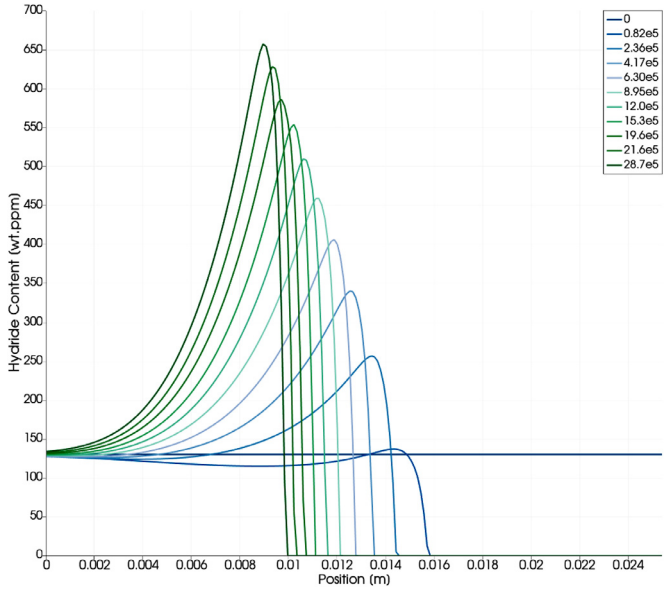

Fig. 7. Evolution of the hydride distribution in Sawatzky's first experiment [13]. A dissolution/precipitation cycle occurring at the limit between the one-phase and two-phase regions creates a hydride peak that gets higher and sharper as time passes. The times in the legend are given in seconds.

Figure 7 shows the evolution of the hydride distribution in the sample. The experiment starts with a uniform hydrogen profile, in which almost all hydrogen is in hydrides at room temperature. As the temperature is increased, the hydrides dissolve on the hot side. The resulting solute hydrogen migrates towards the colder side and build up, creating an increased bump of hydride concentration. Hydrogen migration continues because of the Soret effect, which creates a deficit of hydrogen in solution, so this bump dissolves again and the hydrogen reprecipitates further on the left, forming a higher, sharper hydride peak. This dissolution/precipitation cycle repeats during the whole experiment. If the solubility is higher, the driving force for dissolution is increased, so the dissolution/precipitation cycle repeats itself faster, hence the hydride peak shifts further to the left at the end of the simulation when using a higher solubility fit, as shown in Figure 6.

The simulation of the two experiments shows that the HNGD model is able to predict the hydride profile in a sample initially loaded with a uniform hydrogen profile, and subjected to a temperature gradient. The next set of experiments shows the results when modeling an experiment with an initially inhomogeneous hydrogen distribution in which a hydride rim is present at one end of the sample at the start.

3.2.3. Kammenzind's Shallow Profile Experiments

The third set of cases is from a set of experiments performed by Kammenzind and described by Merlino in [14]. In these experiments, 3.81cm-long Zircaloy samples are hydrogen-loaded via electrolysis, forming a hydride rim at one end of the sample (at $x = 3.81cm$, on the right in Fig. 8). An asymmetric temperature profile is then applied for several months. Table 2 sums up the annealing times and temperatures for each sample. The labels A53, A54, A55a/b and A56 were used to identify the different samples in [14]. The maximum temperature in the samples occurs at position $x \approx 2.5cm$.

When the sample goes from room temperature to annealing temperature, the hydride rim starts dissolving. The hydrogen produced builds up so Fickian diffusion overcomes the Soret effect. When this happens, the hydrogen in solid solution can migrate past the peak temperature spot, and continue toward the colder side. Hydride precipitation occurs in a domain near the cold end (about 0.5 to 1cm wide), with a maximum hydrogen content of a few hundreds of $wt.ppm$ at the interface. At the end of the experiment, the hydride rim has not completely dissolved: the far most right experimental point still reaches 600 to 3000$wt.ppm$ of hydrogen.

Table 2
Summary of the annealing times and temperatures

ID	Anneal Time	T_{left}	T_{max}	T_{right}
A53	150 days	533	644	575
A54	194 days			
A56	95 days			
A55a	209 days	589	644	616
A55b				

To simulate this experiment, the initial condition is built assuming that (i) the hydride rim is made of a solid hydride, (ii) the rest of the sample ('body') contains a small amount of hydrogen, and (iii) at room temperature the concentration of hydrogen in solid solution is negligible (all is precipitated). In the code, this is translated as (i) $C_{prec} = C_{rim} = 17000wt.ppm$ on a certain length δ, (ii) $C_{prec} = C_{body} = 10wt.ppm$ in the rest of the sample, and (iii) $C_{ss} = 0wt.ppm$ everywhere. The value of δ is determined from conservation of mass. The total hydrogen content of the sample H is derived from the experimental data, and δ is defined so that H is constant during the simulation:

$$Experiment: \quad H = \frac{1}{L}\sum_i h_i l_i \tag{13}$$

$$Simulation: \quad H = \frac{1}{L}\int_0^L C_{prec}dx = \frac{(L-\delta)C_{body} + \delta C_{rim}}{L} \tag{14}$$

where h_i and l_i are the hydrogen content and length of the slices cut at the end of the experiment and L is the length of the sample. Using Equations 13 and 14 we obtain:

$$\delta = L\frac{H - C_{body}}{C_{rim} - C_{body}} \tag{15}$$

Figure 8 shows the results of BISON simulations compared with the experimental data. This time the parameter that is modified is the TSS_P fit, similarly to the solubility in the previous case.

In the simulation, the sample temperature is initially at 300K and takes an hour to reach the desired annealing profile. During the annealing, the hydride rim dissolves partially, emitting hydrogen into the rest of the sample. The hydrogen in solid solution migrates to the cold side and builds up at the cold end. If C_{SS} reaches the TSS_P limit, hydride nucleation is triggered in the first node on the left in the simulation mesh (cold end). Then hydride growth also occurs, creating a depletion of hydrogen in solid solution in the first node. With this depletion, and under Fickian and Soret diffusion, the first node acts as a hydrogen sink: the concentration in solid solution reaches TSS_P (equilibrium between the hydrides and the matrix) and all hydrogen that reaches this node is absorbed via hydride growth. Because of this, the hydrogen concentration in the other nodes is lowered and remains below TSS_P. As a result, if precipitation occurs in the first node, it does not occur anywhere else in the simulation domain. Whether precipitation occurs in the first node depends on the choice of the TSS_P fit, as seen in Figure 8. For each sample simulated, the results overlap when using the default TSS_P fit or a higher one. With a lower TSS_P, precipitation can occur in the first node only, if anywhere. The lower TSS_P allows precipitation in all cases, except for the sample A56 for which all profiles overlap. The model fails to predict the hydride profile in the bipha-

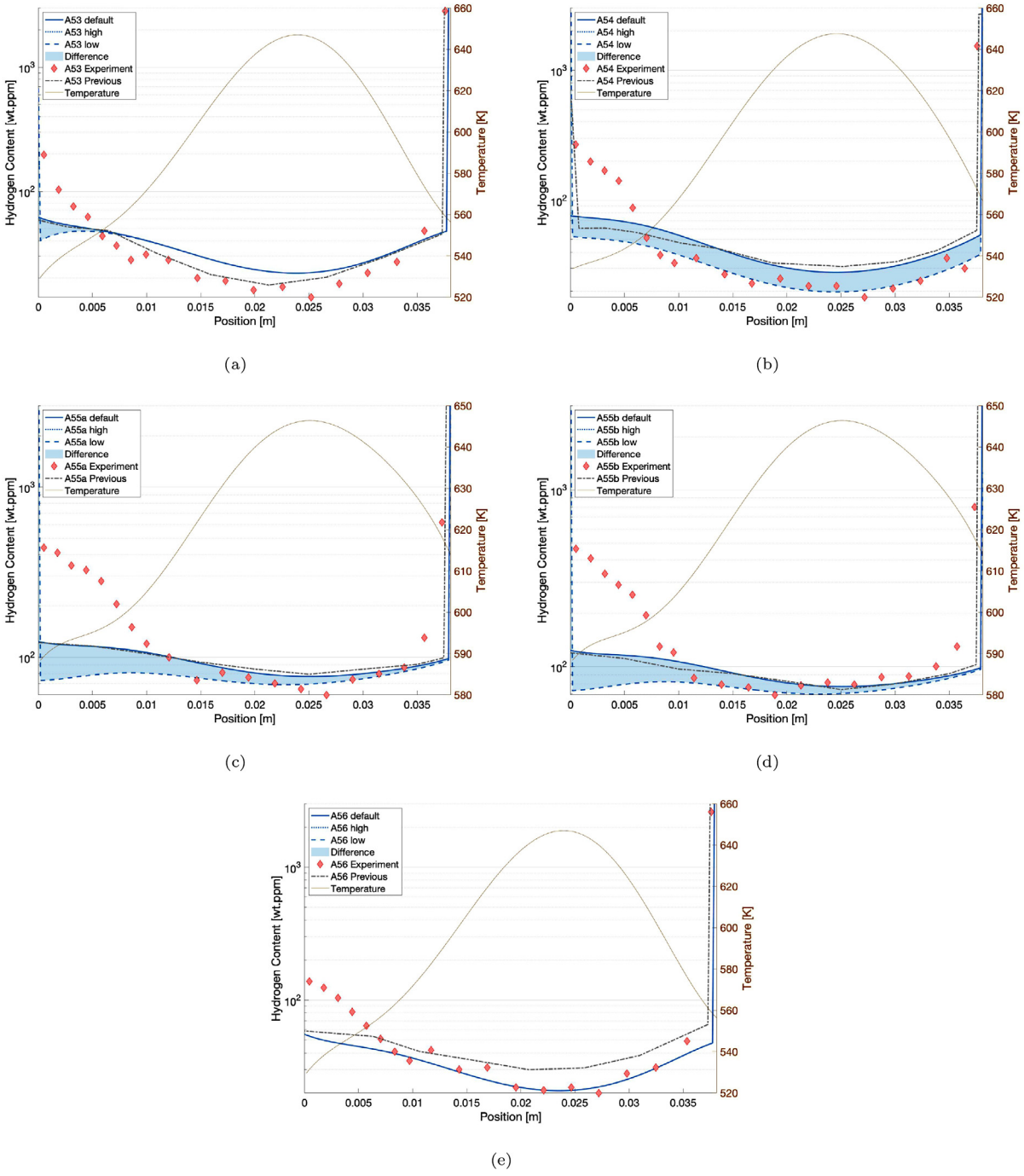

Fig. 8. Simulation of the cases from [14] with three different fits of TSS_P: the default fit of the HNGD model, one standard deviation higher (noted 'high'), and one standard deviation lower (noted 'low'), based on the variability of the TSS_P fits in the litterature [7–12]. TSS_P. The results are similar to those obtained with the previous model.

sic region, which is an issue that already existed with the previous model.

The impact of modifying two of the hydride precipitation parameters is simply shown here, but diffusion parameters also have an important impact as shown by Aly et al. in [15,16]. That study was performed on the previous model, but the diffusion components (Fick's law and Soret effect) were not modified by the HNGD update so the trend may still hold.

4. Conclusion and future work

This study describes the implementation of the Hydride Nucleation-Growth-Dissolution (HNGD) model into the fuel performance code BISON. As part of this work, we have performed systematic verification calculations for each represented physical mechanism, and validation against data from eight experiments.

The calculated hydrogen distribution and hydride precipitation show significant qualitative and quantitative improvement of the model predictions relative to the simple model previously available in BISON. The model is valid for samples containing up to $\sim 300 wt.ppm$ of hydrogen, and it is now available for use by the community of BISON users.

Future work includes predicting the hydrogen profile in experiments where hydrogen is not initially homogeneously distributed.

Declaration of Competing Interest

The authors declare that they have no known competing financial interests or personal relationships that could have appeared to influence the work reported in this paper.

CRediT authorship contribution statement

Florian Passelaigue: Software, Writing - original draft, Visualization. **Evrard Lacroix:** Conceptualization, Methodology, Writing - review & editing. **Giovanni Pastore:** Supervision, Conceptualization, Methodology, Validation, Resources, Writing - review & editing. **Arthur T. Motta:** Supervision, Conceptualization, Validation, Writing - review & editing, Funding acquisition.

Acknowledgements

This work was part of the DOE NEUP Integrated Research Project IRP-17-13708 "Development of a Mechanistic Hydride Behavior Model for Spent Fuel Cladding Storage and Transportation"; we acknowledge helpful discussion with the other members of the IRP project.

The implementation part of this work was mainly achieved through an internship for one of the authors (FP) at Idaho National Laboratory; we acknowledge the help of the BISON team.

The submitted manuscript has been authored by a contractor of the U.S. Government under Contract DE-AC07-05ID14517. Accordingly, the U.S. Government retains a non-exclusive, royalty free license to publish or reproduce the published form of this contribution, or allow others to do so, for U.S. Government purposes.

Supplementary materials

Supplementary material associated with this article can be found, in the online version, at doi:10.1016/j.ijheatmasstransfer.2020.119570.

References

[1] A.T. Motta, L. Capolungo, L.-Q. Chen, M.N. Cinbiz, M.R. Daymond, D.A. Koss, E. Lacroix, G. Pastore, P.-C.A. Simon, M.R. Tonks, B.D. Wirth, M.A. Zikry, Hydrogen in zirconium alloys: A review, Journal of Nuclear Materials 518 (2019) 440–460, doi:10.1016/J.JNUCMAT.2019.02.042.

[2] O. Courty, A.T. Motta, J.D. Hales, Modeling and simulation of hydrogen behavior in Zircaloy-4 fuel cladding, Journal of Nuclear Materials 452 (2014) 311–320, doi:10.1016/J.JNUCMAT.2014.05.013.

[3] D. Stafford, Multidimensional simulations of hydrides during fuel rod life cycle, Journal of Nuclear Materials 466 (2015) 362–372, doi:10.1016/J.JNUCMAT.2015.06.037.

[4] E. Lacroix, P.-C.A. Simon, A.T. Motta, J. Almer, Zirconium hydride precipitation and dissolution kinetics in the hysteresis region in zirconium alloys, ASTM, in press (2019).

[5] E. Lacroix, A. Motta, J. Almer, Experimental determination of zirconium hydride precipitation and dissolution in zirconium alloy, Journal of Nuclear Materials 509 (2018) 162–167, doi:10.1016/J.JNUCMAT.2018.06.038.

[6] M. Avrami, Kinetics of Phase Change. I General Theory, The Journal of Chemical Physics Volume 7 (1939) 1103–1112, doi:10.1063/1.1750380.

[7] J. Kearns, Diffusion coefficient of hydrogen in alpha zirconium, Zircaloy-2 and Zircaloy-4, Journal of Nuclear Materials 43 (1972) 330–338, doi:10.1016/0022-3115(72)90065-7.

[8] A. McMinn, E. Darby, J. Schofield, The Terminal Solid Solubility of Hydrogen in Zirconium Alloys, Zirconium in the Nuclear Industry: Twelfth International Symposium ASTM STP 1354 (2000) 173–195, doi:10.1520/stp14300s.

[9] K. Une, S. Ishimoto, Dissolution and precipitation behavior of hydrides in Zircaloy-2 and high Fe Zircaloy, Journal of Nuclear Materials 322 (2003) 66–72, doi:10.1016/S0022-3115(03)00320-9.

[10] Z. Pan, I. Ritchie, M. Puls, The terminal solid solubility of hydrogen and deuterium in Zr-2.5Nb alloys, Journal of Nuclear Materials 228 (1996) 227–237, doi:10.1016/S0022-3115(95)00217-0.

[11] P. Vizcaino, A. Banchik, J. Abriata, Solubility of hydrogen in Zircaloy-4: irradiation induced increase and thermal recovery, Journal of Nuclear Materials 304 (2002) 96–106, doi:10.1016/S0022-3115(02)00883-8.

[12] K.B. Colas, A.T. Motta, M.R. Daymond, J. Almer, Mechanisms of Hydride Reorientation in Zircaloy-4 Studied in Situ, in: Zirconium in the Nuclear Industry: 17th International Symposium, ASTM STP 1543, ASTM International, 2015, pp. 1107–1137. https://doi.org/10.1520/STP154320120168.

[13] A. Sawatzky, Hydrogen in zircaloy-2: Its distribution and heat of transport, Journal of Nuclear Materials 2 (1960) 321–328, doi:10.1016/0022-3115(60)90004-0.

[14] J. Merlino, Experiments in hydrogen distribution in thermal gradients calculated using bison, M.Eng. paper in Nuclear Engineering, The Pennsylvania State University (2019).

[15] Z. Aly, A. Casagranda, G. Pastore, N.R. Brown, Variance-based sensitivity analysis applied to hydrogen migration and redistribution model in Bison. Part I: Simulation of historical experiments, Journal of Nuclear Materials 524 (2019) 90–100, doi:10.1016/j.jnucmat.2019.06.035.

[16] Z. Aly, A. Casagranda, G. Pastore, N.R. Brown, Variance-based sensitivity analysis applied to the hydrogen migration and redistribution model in Bison. Part II: Uncertainty quantification and optimization, Journal of Nuclear Materials 523 (2019) 478–489, doi:10.1016/j.jnucmat.2019.06.023.